

Folding transitions of the square–diagonal two–dimensional lattice*

Emilio N.M. Cirillo

Dipartimento di Matematica, II Università di Roma – Tor Vergata,
via della Ricerca Scientifica, I–00133 Roma, Italy.

Giuseppe Gonnella

Istituto Nazionale per la Fisica della Materia, Unità di Bari
and Dipartimento di Fisica dell’Università di Bari
and Istituto Nazionale di Fisica Nucleare, Sezione di Bari
via Amendola 173, 70126 Bari, Italy.

Alessandro Pelizzola

Dipartimento di Fisica del Politecnico di Torino
and Istituto Nazionale per la Fisica della Materia,
c. Duca degli Abruzzi 24, 10129 Torino, Italy.

Abstract

The phase diagram of a vertex model introduced by P. Di Francesco (Nucl. Phys. B **525**, 507 1998) representing the configurations of a square lattice which can fold with different bending energies along the main axes and the diagonals has been studied by Cluster Variation Method. A very rich structure with partially and completely folded phases, different disordered phases and a flat phase is found. The crumpling transition between a disordered and the flat phase is first–order. The CVM results are confirmed by the analysis of the ground states and of the two limits where the model reduces to an Ising model.

*PACS numbers: 05.50.+q (Ising problems); 64.60.-i (General studies of phase transitions); 82.65.Dp (Thermodynamics of surfaces and interfaces).

1. Introduction

Polymerized membranes are two-dimensional networks of molecules with fixed connectivity [1]. Their configurational properties and the existence of a crumpling transition between a folded and a flat phase are relevant for the behavior of some biological systems [2]. Models of polymerized membranes can be defined on regular lattices. The constraint of fixed connectivity gives rise to the definition of complicate vertex models which offer the advantage that explicit analytical calculations can be performed [3]. In these models the bonds between the vertices of the network have a fixed length and also, as a further simplification, self-avoidance is not considered. In this way the only degrees of freedom of the network are related to its possible states of folding and each state can be weighted by a Boltzmann factor depending on the relative angle between adjacent plaquettes in the network.

The model studied in this paper has been introduced by Di Francesco [4, 5] and concerns the folding properties of a square lattice which can be folded along the main axes and along the diagonals. This model follows previous studies of the folding properties of a triangular network embedded in d -dimensional lattices. In the case $d = 2$ [6, 7] each triangle of the network can be only in a “up” or “down” state. The entropy of this problem is the same as in the three-colouring problem of the honeycomb lattice [8]. The introduction of a bending rigidity induces a first-order crumpling transition which has been studied in [9, 10]. The model with the triangular network embedded in the face-centered-cubic lattice was defined in [11] and a first-order transition has been found also in this case [12, 13].

In this paper we consider the two-dimensional folding of the square-diagonal lattice and study the phase diagram of this system in terms of the bending rigidities κ_S and κ_L relative to short and long edges. Actually, the phase behavior of this model was already considered in [5] by means of a transfer matrix analysis, but the ground state was not properly investigated, and as a consequence some phases were missing. Here we consider the complete set of the ground states of the model and study the phase diagram at finite temperatures by the cluster variation method (CVM) [14, 15, 16, 17]. This method has already proven to be useful for studying vertex models and folding problems [10, 12, 13].

The outline of the paper is the following. In the next Section we define the model; the ground states will be shown in Section 3. In Section 4 the CVM approximation used in this paper will be described and our results will be presented in Section 5.

2. The square-diagonal folding model

We consider the folding configurations of the square-diagonal lattice where any couple of adjacent triangles can be on the same plane or with the two triangles one on the other. Triangles can be folded with respect to the main axes of the square lattice or with respect to the diagonals so that in the definition of the bending energy different couples of triangles with a short edge or a long edge in common have to be considered. We will start the definition of the model by enumerating the folding states in terms of loop configurations.

2.1. Folding and loop configurations

First fix a reference orientation for all the edges of the lattice in such a way that for each triangle the vectorial sum of the oriented edges is zero. There are two choices for this global orientation and one is shown in Fig. 1. In any folding configuration each short edge is mapped on one of the four vectors $\pm\vec{e}_1, \pm\vec{e}_2$; this mapping defines the state of the network. Then consider two triangles with a long edge in common as the pair shaded in Fig. 1. This pair can be in two folding states that can be represented in the following way: consider another square lattice as in Fig. 2. The lines joining the centers of the edges are dashed or full depending on whether they are dual to the mapped short edge vectors $\pm\vec{e}_1$ or $\pm\vec{e}_2$ respectively. The obvious observation that in each triangle there is a short edge vector in the direction of $\pm\vec{e}_1$ and an edge in the direction of $\pm\vec{e}_2$ implies that for each center of the edges of the new square lattice there will be two dashed and two full lines. As a consequence the dashed lines and the full lines will form two sets of orthogonal closed loops [4].

Taking into account also the orientation of \vec{e}_1 and \vec{e}_2 , it comes out that each closed loop has its own orientation independently from the others. Therefore the original folding problem is equivalent to a dense two-loop problem where a sign representing the orientation has to be attributed to each closed loop. Further details can be found in [4].

Consider now the square plaquettes of this new lattice. In each plaquette there are two dashed and two full lines. On each line there can be two possible signs so that there are $2 \times 2^4 = 32$ states for each plaquette. Of course, the sign conservation law along the closed loops implies that only some of the 32^2 configurations of two neighboring plaquettes are allowed. The logarithm of the number of all possible states of these plaquette configurations gives the entropy of the folding problem.

2.2. Bending energy

Here we introduce a bending energy weighting the different folding configurations. We attribute a Boltzmann weight e^{κ_L} or $e^{-\kappa_L}$ respectively to each unfolded or folded long edge. Similar weights $e^{\pm\kappa_S}$ are associated to the two short edge folding states.

In the plaquette formulation long and short edge bending energies appear in an asymmetric way. Long edge bending energy results in an interaction between each couple of adjacent plaquettes in the loop formulation. An energy $-\kappa_L$ has to be assigned to the network any time a dashed line (or equivalently a full line) crosses the edge between two plaquettes without bending. In the other case an energy κ_L has to be assigned to any right angle of dashed lines between neighboring plaquettes (see Fig. 2).

Differently, short edge bending energy results in different weights for the 32 basic plaquette configurations. In the reference orientation state of Fig. 1, in each square the two short edges on the same diagonal always have opposite orientations. These two short edges acquire the same sign for each folding relative to their perpendicular diagonal. In this case two triangles are folded and an energy $2\kappa_S$ has to be assigned to the network. In the loop formulation this is equivalent to have a couple of parallel lines in one plaquette with the same sign. Similar considerations hold for an unfolded edge and for the other couple of parallel lines in a plaquette. Therefore, in total, each plaquette can have an energy equal to $-4\kappa_S$, 0, or $4\kappa_S$ [5].

2.3. The vertex representation

From the discussion above it is clear that our model can be thought as a vertex model defined on a two-dimensional square lattice \mathbb{Z}^2 . A vertex variable $\sigma_x \in \{1, \dots, 32\}$ is associated to each site x of the lattice; to each value of σ_x corresponds one of the 32 vertices introduced above (a possible representation is shown in Fig. 3).

Constraints between neighboring vertices are implied by the sign conservation law along the closed loops. By using the labelling of Fig. 3 these constraints can be written in a simple form: we define the two 32×32 matrices $\mu^h(\sigma, \sigma') = \delta_{u_2(\sigma), u_4(\sigma')}$ and $\mu^v(\sigma, \sigma') = \delta_{u_3(\sigma), u_1(\sigma')}$ where $\sigma, \sigma' \in \{1, \dots, 32\}$ and $u(\sigma)$ is the vector u associated to the vertex σ . A configuration $\bar{\sigma} = \{\sigma_x\}_{\mathbb{Z}^2}$ is allowed if $\mu^h(\sigma_x, \sigma_y) = 1$ and $\mu^v(\sigma_x, \sigma_y) = 1$ respectively for any horizontal, $\langle x, y \rangle_h$, and vertical, $\langle x, y \rangle_v$, pair of nearest neighboring sites. Notice that on each bond there are only 256 allowed configurations out of the $32^2 = 1024$ total ones. We remark that when we write $\langle x, y \rangle_{h,v}$ we suppose the sites x and y lexicographically ordered.

The hamiltonian of the model is in the form

$$H(\bar{\sigma}) = \sum_{x \in \mathbb{Z}^2} H^s(\sigma_x) + \sum_{\langle x, y \rangle_h} H^h(\sigma_x, \sigma_y) + \sum_{\langle x, y \rangle_v} H^v(\sigma_x, \sigma_y) \quad , \quad (2.1)$$

where the two body potential is given by the two 32×32 matrices $H^v(\sigma', \sigma) = H^h(\sigma, \sigma') = 2\kappa_L \delta_{v(\sigma), 1-v(\sigma')} - \kappa_L$ for any $\sigma, \sigma' \in \{1, \dots, 32\}$ and the single body potential is given by the vector $H^s(\sigma) = 4\kappa_S$ if $\sigma = 1, \dots, 8$, $H^s(\sigma) = -\kappa_S$ if $\sigma = 25, \dots, 32$ and $H^s(\sigma) = 0$ otherwise. Finally we can write the partition function of the model:

$$Z(\kappa_S, \kappa_L) = \sum_{\bar{\sigma}} \left(\prod_{\langle x, y \rangle_h} \mu^h(\sigma_x, \sigma_y) \prod_{\langle x, y \rangle_v} \mu^v(\sigma_x, \sigma_y) \right) \exp\{-H(\bar{\sigma})\} \quad , \quad (2.2)$$

where the inverse temperature β has been adsorbed in the hamiltonian.

3. Ground states

The ground states of the network can be conveniently discussed in terms of loop configurations. First consider what happens for $\kappa_S, \kappa_L > 0$ at very low temperatures. A large positive κ_L selects states with straight lines so that in a square lattice with periodic boundary conditions there are the dashed and full closed loop shown in Fig. 4(a). A positive value of κ_S favors alternate sign values on these lines. This corresponds to a completely flat state with an energy per plaquette given by $E_1 = -4\kappa_S - 2\kappa_L$. There are 8 possible degenerate ground states of this kind and each of them can be realized with two basic plaquette states.

In the sector $\kappa_S < 0, \kappa_L > 0$ elementary triangles want to be folded along diagonals. A positive value of κ_L still select straight lines. All the dashed lines have one sign and the same for the full lines. The network is in a state where two triangles sharing a long edge are on the same plane and all the other triangles are

above one of those two. Also in this case the degeneracy is 8 while one plaquette state is enough for building the global state which has an energy $E_2 = 4\kappa_S - 2\kappa_L$ per plaquette and is reported in Fig. 4(b).

Loop-configuration ground states for the remaining sectors $\kappa_S < 0, \kappa_L < 0$ and $\kappa_S > 0, \kappa_L < 0$ are respectively shown in Fig. 4(c) and Fig. 4(d). They have an energy equal to $E_3 = 4\kappa_S + 2\kappa_L$ and $E_4 = -4\kappa_S + 2\kappa_L$. They describe a completely folded state with all triangle one above the other, and a state with four triangles with a common vertex on the same plane and all other triangles folded above. There are needed 2 and 4 different plaquettes for building up ground states in sectors 3 and 4 respectively.

4. The CVM approximation

In this section we describe the CVM approximation we used to study the phase diagram of model (2.2). We do not enter into all the details related to the CVM technique, we just refer to [14, 15, 16].

The CVM is based on the minimization of the free-energy density functional obtained by a truncation of the cluster (cumulant) expansion of the corresponding functional appearing in the exact variational formulation of statistical mechanics. The existence of different horizontal and vertical interactions in the hamiltonian (2.1) and the structure of the ground states of the model suggest that one should consider at least a square (four-vertex) approximation, that is one should consider a square of four vertices as the largest cluster in the expansion of the free-energy functional. Moreover, in order to reproduce the structure of the ground states we are forced to partition our lattice into four square lattices with spacing two (see Fig. 5). We denote by A, B, C and D these four sublattices and we introduce four square density matrices: $\rho_{ABCD}, \rho_{BAD C}, \rho_{CDAB}$ and ρ_{DCBA} . We also need four pair density matrices $\rho_{AB}, \rho_{BA}, \rho_{CD}$ and ρ_{DC} for the four horizontal different bonds, four pair density matrices $\rho_{AC}, \rho_{CA}, \rho_{BD}$ and ρ_{DB} for the four different vertical bonds and four single site matrices ρ_A, ρ_B, ρ_C and ρ_D . Finally, we define the sets $\mathcal{P} = \{ABCD, BADC, CDAB, DCBA\}$, $\mathcal{L}^h = \{AB, BA, CD, DC\}$, $\mathcal{L}^v = \{AC, CA, BD, DB\}$ and $\mathcal{S} = \{A, B, C, D\}$, and we write the free-energy functional per plaquette as follows:

$$\begin{aligned}
f(\{\rho_X : X \in \mathcal{P}\}) &= \frac{1}{4} \sum_{X \in \mathcal{L}^h} \text{Tr}_X [\rho_X H^h] + \frac{1}{4} \sum_{X \in \mathcal{L}^v} \text{Tr}_X [\rho_X H^v] + \frac{1}{4} \sum_{X \in \mathcal{S}} \text{Tr}_X [\rho_X H^s] \\
&+ \frac{1}{4} (\sum_{X \in \mathcal{P}} \text{Tr}_X [\rho_X \log \rho_X] - \sum_{X \in \mathcal{L}^h} \text{Tr}_X [\rho_X \log \rho_X] \\
&- \sum_{X \in \mathcal{L}^v} \text{Tr}_X [\rho_X \log \rho_X] + \sum_{X \in \mathcal{S}} \text{Tr}_X [\rho_X \log \rho_X]) \\
&+ \sum_{X \in \mathcal{P}} \lambda_X (\text{Tr} [\rho_X] - 1)
\end{aligned} \tag{4.1}$$

where λ_X , with $X \in \mathcal{P}$, are four Lagrange multipliers ensuring that ρ_X with $X \in \mathcal{P}$ are correctly normalized and for any $X \in \mathcal{P} \cup \mathcal{L}^h \cup \mathcal{L}^v \cup \mathcal{S}$ we have denoted by Tr_X the sum over all the allowed configurations on the set X .

Following the recipe of the CVM one should find the densities $\{\rho_X : X \in \mathcal{P}\}$ that minimize the functional (4.1). Hence the next step consists in taking derivatives of the free energy with respect to the square densities. In order to do this we must take into account that bond and single site densities can be obtained from square densities via a partial tracing. Namely,

$$\begin{aligned}
\rho_{AB} &= \text{Tr}_{CD} \rho_{ABCD} & \rho_{BA} &= \text{Tr}_{DC} \rho_{BAD C} & \rho_{CD} &= \text{Tr}_{AB} \rho_{CDAB} & \rho_{DC} &= \text{Tr}_{BA} \rho_{DCBA} \\
\rho_{AC} &= \text{Tr}_{BD} \rho_{ABCD} & \rho_{BD} &= \text{Tr}_{AC} \rho_{BAD C} & \rho_{CA} &= \text{Tr}_{DB} \rho_{CDAB} & \rho_{DB} &= \text{Tr}_{CA} \rho_{DCBA} \\
\rho_A &= \text{Tr}_B \rho_{AB} & \rho_B &= \text{Tr}_B \rho_{BA} & \rho_C &= \text{Tr}_D \rho_{CD} & \rho_D &= \text{Tr}_D \rho_{DC}
\end{aligned} \tag{4.2}$$

Actually, each bond or single site density can be derived via partial tracing of different higher order densities. This means that suitable Lagrange multiplier must be introduced to ensure that different partial tracings lead to the same result. More precisely, each bond belongs to two different squares (see Fig. 5): we have to associate a family of multiplier to each bond to ensure that the same result is obtained by tracing over the two plaquettes sharing the bond itself (for instance, we need $\text{Tr}_{CD} \rho_{ABCD} = \text{Tr}_{CD} \rho_{CDAB}$). We get eight different families $\{\lambda_X : X \in \mathcal{L}^h \cup \mathcal{L}^v\}$ and each family contains 256 different multipliers, one for each allowed bond configuration. Moreover, there exist four different bonds sharing the same single site: to each site we associate three different multiplier families $\{\lambda_{X,i} : X \in \mathcal{S}, i = 1, 2, 3\}$, each of them made of 32 different multipliers. Hence we have 20 different families of multipliers resulting in a total number of $8 \times 256 + 12 \times 32 = 2432$ multipliers.

The functional that we have to minimize is no more the free energy (4.1), but the one in which all the Lagrange multipliers are introduced:

$$g(\{\rho_X : X \in \mathcal{P}\}) = 4f(\{\rho_X : X \in \mathcal{P}\}) + \text{Tr}_A [\lambda_{A,1} \text{Tr}_B [\rho_{BA} - \rho_{AB}]] + \dots \dots \dots + \text{Tr}_{AB} [\lambda_{AB} \text{Tr}_{CD} [\rho_{CDAB} - \rho_{ABCD}]] + \dots \dots \dots \quad (4.3)$$

where dots stand for other seven similar bond terms and eleven similar single site terms. Now, let us label with $\alpha \in \{1, \dots, 4608\}$ the allowed 4608 square states. We denote by $\sigma_X(\alpha)$ the vertex associated to the site $X \in \mathcal{S}$ corresponding to α . To obtain the equilibrium densities we have to set equal to zero the derivatives of the functional (4.3) taken with respect to $\rho_Y(\alpha)$ with $Y \in \mathcal{P}$ and $\alpha \in \{1, \dots, 4608\}$. In the case $Y = ABCD$ we obtain:

$$\begin{aligned} \rho_{ABCD}(\alpha) = & \text{const} \times \exp \left\{ -H^h(\sigma_A(\alpha), \sigma_B(\alpha)) - H^v(\sigma_A(\alpha), \sigma_C(\alpha)) - H^s(\sigma_A(\alpha)) \right. \\ & + \lambda_{AB}(\sigma_A(\alpha), \sigma_B(\alpha)) - \lambda_{CD}(\sigma_C(\alpha), \sigma_D(\alpha)) + \lambda_{AC}(\sigma_A(\alpha), \sigma_C(\alpha)) \\ & - \lambda_{BD}(\sigma_B(\alpha), \sigma_D(\alpha)) + \lambda_{A,1}(\sigma_A(\alpha)) + \lambda_{A,2}(\sigma_A(\alpha)) - \lambda_{B,1}(\sigma_B(\alpha)) \\ & \left. - \lambda_{B,3}(\sigma_B(\alpha)) - \lambda_{C,2}(\sigma_C(\alpha)) + \lambda_{C,3}(\sigma_C(\alpha)) \right\} \\ & \times \rho_{AB}(\sigma_A(\alpha), \sigma_B(\alpha)) \rho_{AC}(\sigma_A(\alpha), \sigma_C(\alpha)) \rho_A(\sigma_A(\alpha))^{-1} \end{aligned} \quad (4.4)$$

The equation above is actually a set of 4608 equations. Three similar sets can be found by considering the cases $X \in \{BADC, CDAB, DCBA\}$. The complete set of $4 \times 4608 = 18432$ equations, together with the equations for the multipliers, can be solved by means of the natural iteration method [18, 19]. The equations for the multipliers can be obtained by taking derivatives of (4.3) with respect to the multipliers and are of the form

$$\lambda_X(\sigma_X) = \lambda_X(\sigma_X) + \text{const} \log \frac{\varphi_1(\sigma_X)}{\varphi_2(\sigma_X)} \quad (4.5)$$

where $X \in \mathcal{L}^h \cup \mathcal{L}^v \cup \mathcal{S}$, σ_X is an allowed configuration on X and φ_1 and φ_2 are linear combinations of higher order densities on clusters $Y \supset X$ traced over $Y \setminus X$.

5. Phase diagram

The phase diagram of the model, as predicted by our approximation, has been reported in Fig. 6, where open symbols denote second order transitions, and full symbols denote first order transitions. The transition lines have been drawn using a limited number of points, since the precise determination of such points is a very computationally demanding task. In particular, the transitions between the phase **D1** (Disordered 1) and the phases **F** (Folded) and **LF** (L-Folded) have been simply sketched since it was possible to determine their location only with a rough approximation.

Several phases appear in the diagram. First of all we have four long-range ordered phases corresponding to the four possible ground states described in Section 3. Phase **F1** (Flat) is stable for large and positive κ_S and κ_L and represents a flat phase. Phase **SF** (S-Folded) is stable for large enough absolute values of $\kappa_S < 0$ and $\kappa_L > 0$. It represents a partially folded phase in which folding occurs mainly along short edges. Phase **F** is stable for large enough absolute values of $\kappa_S < 0$ and $\kappa_L < 0$. It represents a completely folded phase. Phase **LF** is stable for large enough absolute values of $\kappa_S > 0$ and $\kappa_L < 0$. It represents a partially folded phase in which folding occurs mainly at long edges. Like the corresponding ground states, all these phases have degeneracy 8.

On the high temperature side of the ordered flat phase **F1** we have a small slice of the disordered phase **D2** (Disordered 2). In the central part of the phase diagram, we have the disordered phase **D1**, which has larger entropy and larger energy than **D2**. It is noteworthy that the entropy of this phase at the infinite temperature point $\kappa_S = \kappa_L = 0$ is $S_\infty \simeq 0.9204$ in our approximation, while the estimate in [4], obtained by transfer matrix methods, corresponds, with our definitions, to $S_\infty \simeq 0.9196$.

Between phases **SF** and **F** we have the partially ordered phase **PO** (Partially Ordered). For large negative κ_S the transitions between this phase and phases **SF** and **F** tend asymptotically to $|\kappa_L| = \frac{1}{2} \ln \frac{5+\sqrt{17}}{4} \simeq 0.412$,

which is exactly the estimate for the critical coupling of the square lattice Ising model in the present approximation [14]. This is a consequence of a property of the model, which reduces to a square lattice Ising model in the limit $\kappa_S \rightarrow -\infty$. In the loop gas formulation, $\kappa_S \rightarrow -\infty$ implies that all loops in the same set (that is, all dashed loops, or all full loops) must have the same sign. Looking at Fig. 3 one can verify that to satisfy this condition the state of the system must be a mixture of only 2 out of the 32 plaquette states. For this pair of allowed states there are four different possibilities (and thus the phase **PO** has degeneracy 4): (1,5) (corresponding to + signs on both loop sets), (2,6) (+ on full loops and - on dashed loops), (3,7) (- on both loop sets) and (4,8) (- on full loops and + on dashed loops). Hence we have the breaking of the loop sign inversion symmetry, which is restored only at the transition to the phase **5**. Given a pair of allowed states, the hamiltonian reduces to an ordinary Ising hamiltonian, with equal states on adjacent plaquettes giving a contribution $-\kappa_L$ to the total energy, and different states giving $+\kappa_L$. It is therefore an exact result that, in the limit $\kappa_S \rightarrow -\infty$, there must exist the three phases **SF**, **F** and **PO** (corresponding respectively to the ferromagnetic, antiferromagnetic and disordered phases of the Ising model), separated by second order phase transitions at $|\kappa_{Lc}| = \frac{1}{2} \ln(1 + \sqrt{2}) \simeq 0.441$.

A similar situation occurs in the limit $\kappa_L \rightarrow -\infty$. Looking at Fig. 4 one sees that in this limit both the full and the dashed lines form the smallest possible square loops. It follows that the model reduces to two decoupled Ising models, where the Ising variables are the loop signs and two loops (both full, or both dashed) having parallel edges in the same plaquette interact with an energy $\pm 2\kappa_S$. Therefore the phases **F** and **LF** (corresponding respectively to the antiferromagnetic and ferromagnetic phases of the limiting Ising model) will undergo second order phase transitions towards the disordered phase **D1** at $|\kappa_{Sc}| = \frac{1}{4} \ln(1 + \sqrt{2}) \simeq 0.220$. The estimate for this value in our approximation is of course $|\kappa_L| = \frac{1}{4} \ln \frac{5+\sqrt{17}}{4} \simeq 0.206$.

Comparing our phase diagram with that by Di Francesco [5] one can see several striking differences. First of all, among our ordered phases, only the completely flat and completely folded ones were reported in [5], and no low temperature transition was found among them. In addition, no intermediate phase (like our phases **PO** and **D2**) was found between the ordered and the disordered phases. We note that the CVM results are fully confirmed by the ground states analysis and the limits $\kappa_S \rightarrow -\infty$ and $\kappa_L \rightarrow -\infty$.

In conclusions, we have shown that the CVM techniques can be adapted to study very complex vertex models as the one considered in this paper representing the folding configurations of a square-diagonal lattice. As in the case of the folding of the triangular lattice, a first-order crumpling transition between the flat phase and a disordered phase has been found. The extension of this analysis to the d -dimensional folding problem appears not easy from a numerical point of view.

Acknowledgements

G.G. acknowledges support by MURST (COFIN97). E.C. wishes to express his thanks to the European network "Stochastic Analysis and its Applications" ERB-FMRX-CT96-0075 for financial support.

References

- [1] See, e.g., *Statistical Mechanics of Membranes and Surfaces*, edited by D.R. Nelson, T. Piran, and S. Weinberg, (World Scientific, Singapore, 1989).
- [2] D.R. Nelson and L. Peliti, *J. Phys. (France)* **48**, 1085 (1987).
- [3] See, e.g., M. Bowick, P. Di Francesco, O. Golinelli and E. Guitter, *Proceedings of the 4th meeting on “Condensed Matter and High Energy Physics”* ((World Scientific, Singapore, 1997).
- [4] P. Di Francesco, *Nucl. Phys. B* **525**, 507 (1998).
- [5] P. Di Francesco, *Nucl. Phys. B* **528**, 453 (1998).
- [6] Y. Kantor and M.V. Jarić, *Europhys. Lett.* **11**, 157 (1990).
- [7] P. Di Francesco and E. Guitter, *Europhys. Lett.* **26**, 455 (1994).
- [8] R.J. Baxter, *J. Math. Phys.* **11**, 3 (1970).
- [9] P. Di Francesco and E. Guitter, *Phys. Rev. E* **50**, 4418 (1994).
- [10] E.N.M. Cirillo, G. Gonnella and A. Pelizzola, *Phys. Rev. E* **53**, 1479 (1996).
- [11] M. Bowick, P. Di Francesco, O. Golinelli and E. Guitter, *Nucl. Phys. B* **450**, 463 (1995).
- [12] E.N.M. Cirillo, G. Gonnella and A. Pelizzola, *Phys. Rev. E* **53**, 3253 (1996).
- [13] M. Bowick, O. Golinelli, E. Guitter, and S. Mori, *Nucl. Phys. B* **495**, 583 (1997).
- [14] R. Kikuchi, *Phys. Rev* **81**, 988 (1951).
- [15] G. An, *J. Stat. Phys.* **52**, 727 (1988);
- [16] T. Morita, *J. Stat. Phys.* **59**, 819 (1990).
- [17] For a recent review see the volume *Progr. Theor. Phys. Suppl.* **115** (1994).
- [18] R. Kikuchi, *J. Chem. Phys.* **60**, 1071 (1974).
- [19] R. Kikuchi, *J. Chem. Phys.* **65**, 4545 (1976).

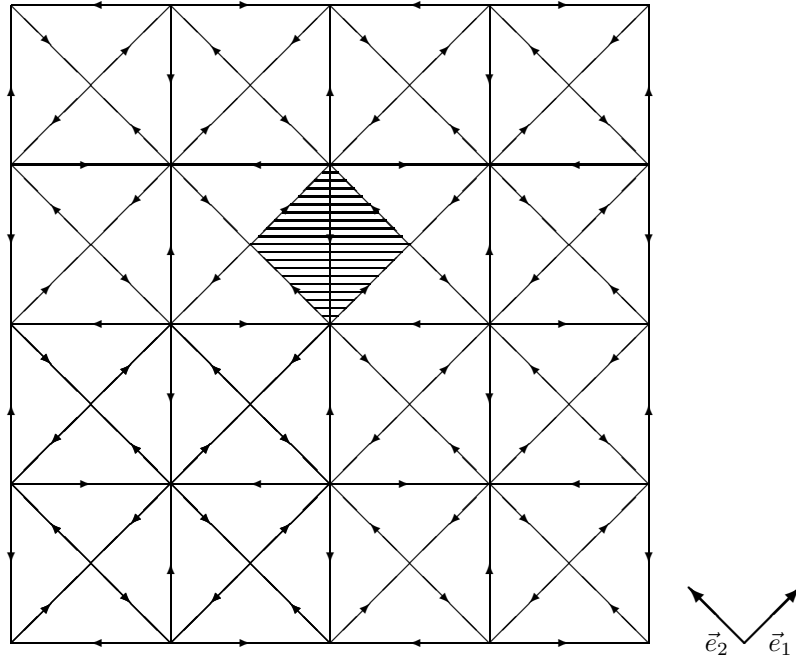


Fig. 1: The square-diagonal lattice.

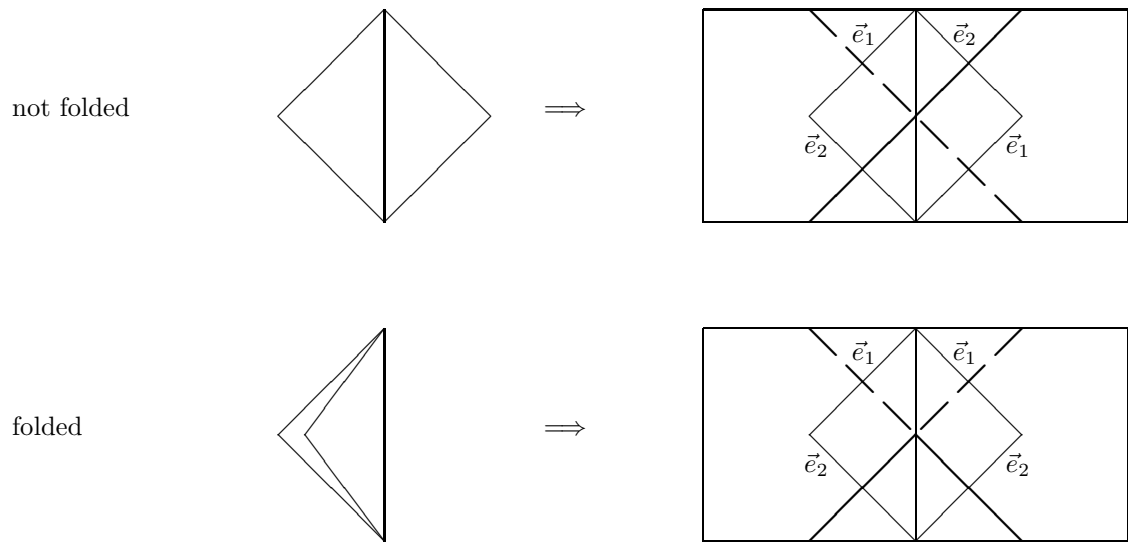


Fig. 2: The mapping onto the vertex model.

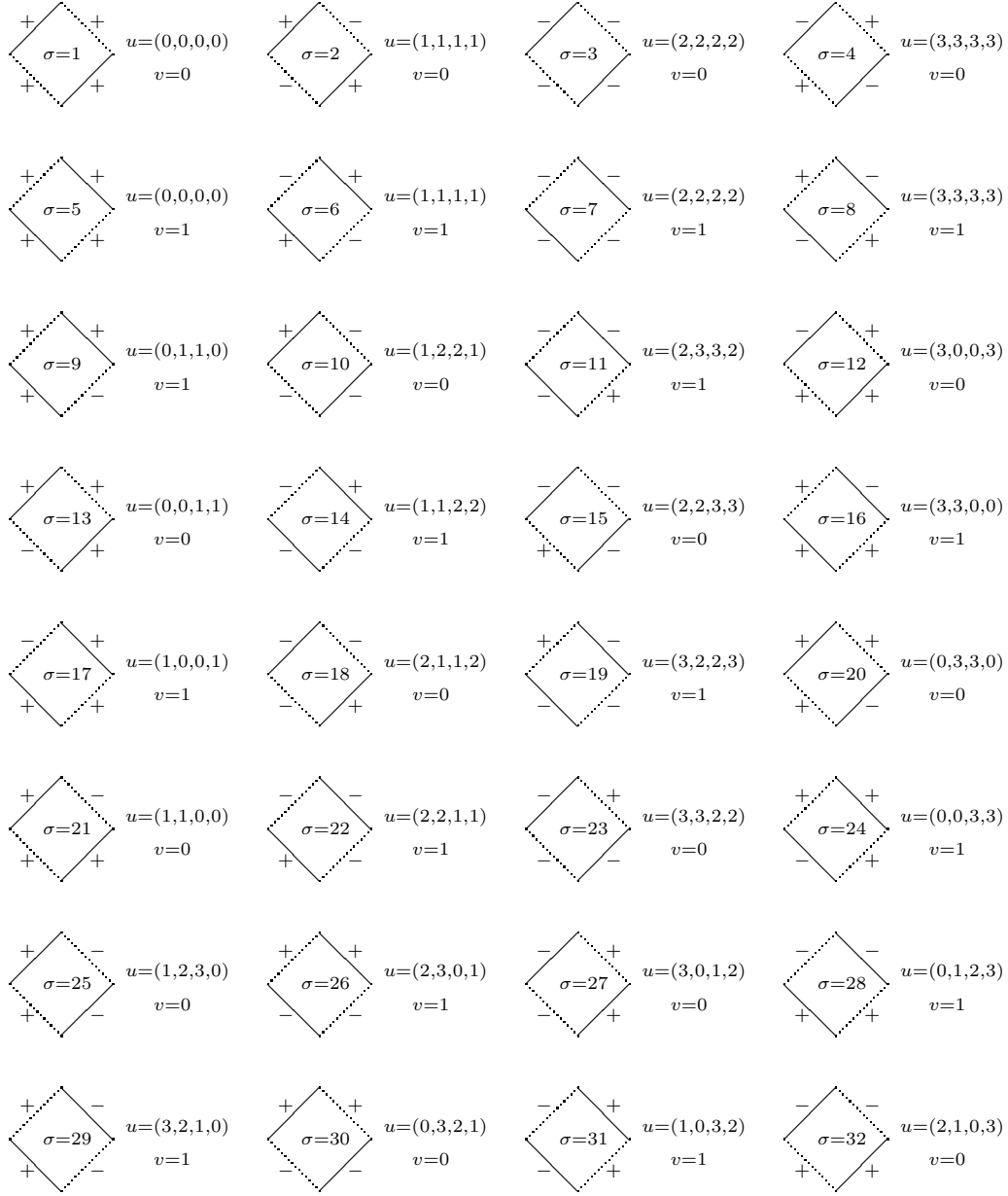
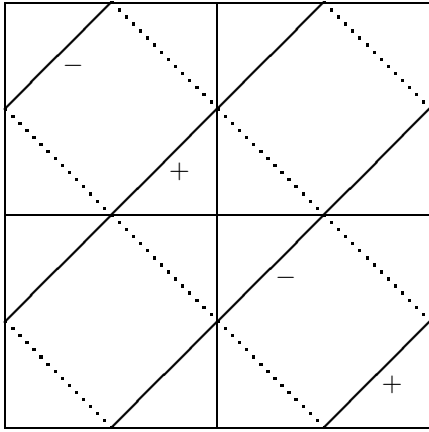
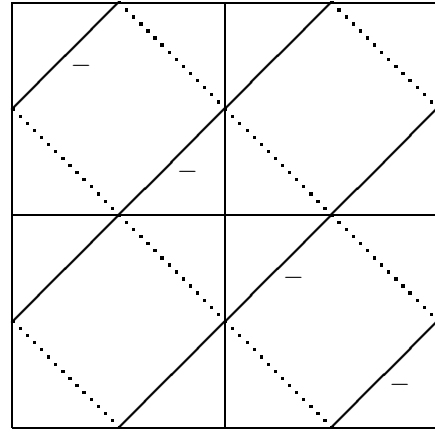


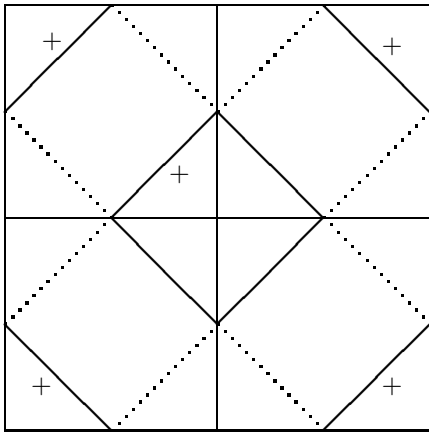
Fig. 3: A possible representation of the vertex variables. Each vertex is labelled by a variable $\sigma \in \{1, \dots, 32\}$. Following [5] a vector $u = (u_1, u_2, u_3, u_4) \in \{0, 1, 2, 3\}^4$ and a scalar $v \in \{0, 1\}$ are associated to any $\sigma \in \{1, \dots, 32\}$ (see [4] for more details).



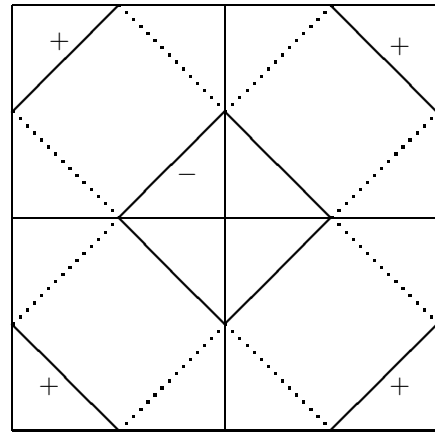
(a)



(b)



(c)



(d)

Fig. 4: The ground states depicted in figures (a), (b), (c) and (d) correspond, respectively, to the phases **F1**, **SF**, **F** and **LF** in Fig. 6.

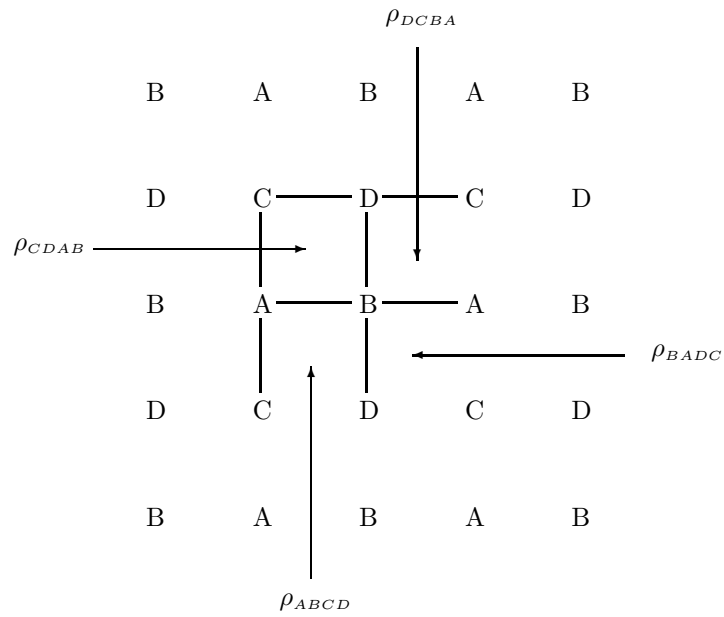


Fig. 5: Partition of the lattice used in the CVM calculation. The eight bonds and the four plaquettes are explicitly depicted.

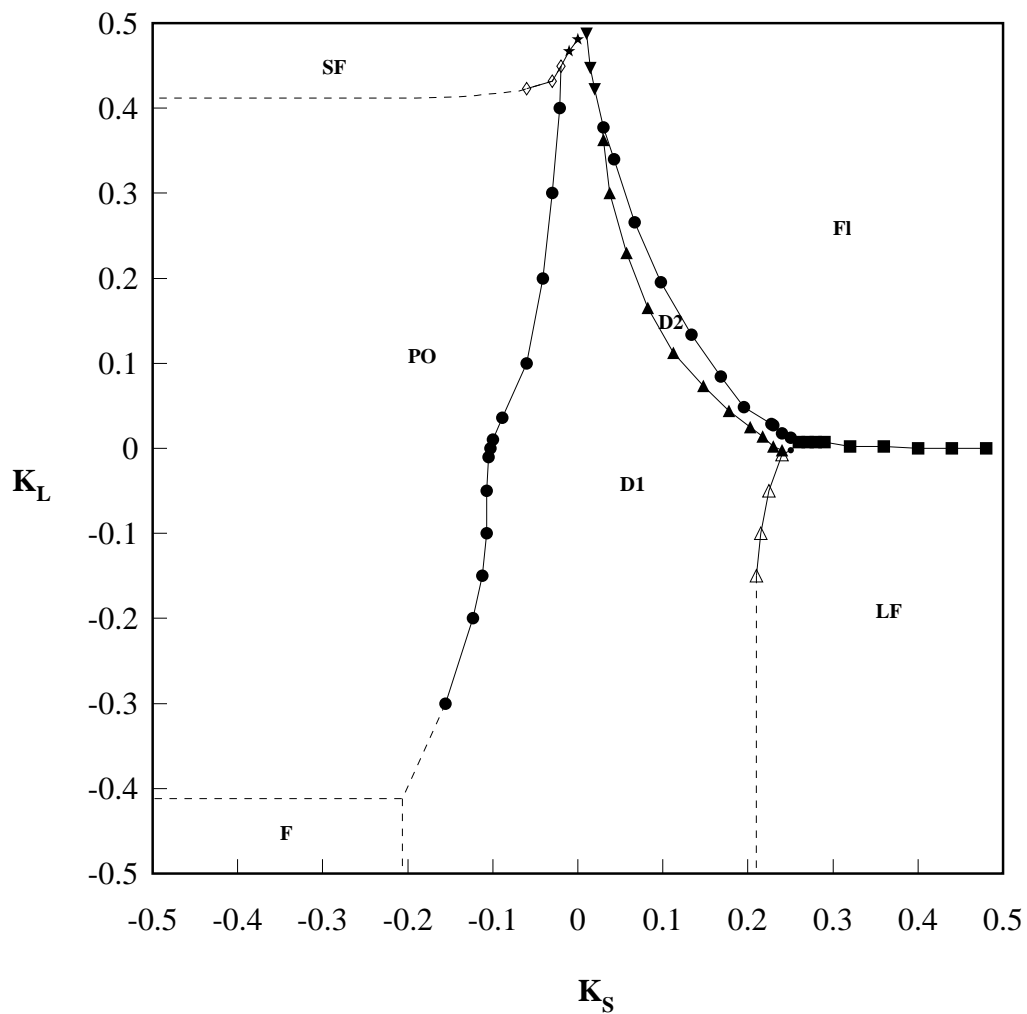


Fig. 6: The phase diagram: open (full) symbols denote second (first) order transition points calculated via CVM. Solid lines are eye-guides, dashed lines are suggested by the limits $\kappa_S, \kappa_L \rightarrow \infty$.